Chapter 2

IGM heating due to primordial magnetic fields during cosmic dawn*

The primordial magnetic field is a tantalizing clue to the physics of the early universe, and a window into the processes that shaped the cosmos we observe today.

– J. Richard Bond

The global redshifted HI 21-cm signal from the dark ages and cosmic dawn is a promising tool to study the primordial magnetic field (see Subramanian, 2016, for a review). The primordial magnetic field can heat up the Hydrogen and Helium gas in

*This chapter is adapted from the paper, "Primordial magnetic fields during the cosmic dawn in light of EDGES 21-cm signal" by Bera, Datta, and Samui (2020).

the intergalactic medium by processes such as the ambipolar diffusion (AD) and decaying turbulence (DT) (Jedamzik, Katalinić, and Olinto, 1998; Subramanian and Barrow, 1998; Kunze and Komatsu, 2014; Chluba et al., 2015). This indirectly affects the spin temperature and the globally averaged redshifted HI 21-cm signal (Sethi, 2005). Furthermore, the growth of structures during the cosmic dawn gets accelerated in presence of magnetic field in the IGM. As a consequence, the primordial magnetic field can have an important impact on the formations of the first luminous sources (Sethi, Nath, and Subramanian, 2008; Schleicher, Banerjee, and Klessen, 2008). A substantial amount of theoretical work has been carried out to understand, in detail, the role of the primordial field on the HI 21-cm signal (Tashiro and Sugiyama, 2006; Schleicher, Banerjee, and Klessen, 2009; Venumadhav et al., 2017; Kunze, 2019), early structure formation during the cosmic dawn and reionization (Kim, Olinto, and Rosner, 1996; Yamazaki et al., 2006; Pandey et al., 2015).

The measurements of the global HI 21-cm absorption signal by the EDGES experiments in the redshift range $z \sim 14$ to 20 (Bowman et al., 2018a) have opened up a possibility to constrain the primordial magnetic field and understand its evolution during the cosmic dawn and dark ages. The details of this observation are given in the previous chapter. In a recent work, Minoda, Tashiro, and Takahashi (2019) has exploited the EDGES data to put an upper limit on the primordial magnetic field. The analysis has been carried out on the backdrop of the standard cosmological model and baryonic interactions of the IGM. However, the measured EDGES absorption signal is $\sim 2-3$ times stronger compared to predictions by the standard model. If the measurements are confirmed, one promising way to explain the measured signal is to consider the IGM to be significantly 'colder' compared to the IGM kinetic temperature predicted by the standard scenario. As mentioned before, one needs to consider a non-standard cooling mechanism such as the DM-baryon interaction in order to make the IGM colder (Tashiro, Kadota, and Silk, 2014; Muñoz, Kovetz, and Ali-Haïmoud, 2015).

In this chapter, we present the constraints on the primordial magnetic field using

the EDGES 21-cm absorption profile on the backdrop of the colder IGM scenario. We consider interactions between cold DM particles and baryons (Tashiro, Kadota, and Silk, 2014; Muñoz, Kovetz, and Ali-Haïmoud, 2015) which makes the IGM colder as compared to that in the standard predictions. If one considers DM-baryon interaction in order to make the IGM colder, the exact constraints on the primordial magnetic field should also depend on the mass of the DM particles and the interaction cross-section between the DM particles and baryons. Thus, it is important to highlight these aspects in order to understand the role of the primordial magnetic field on the 21-cm absorption signal and put limits on the primordial magnetic field. Recently, Bhatt, Jitesh R. et al. (2020) has used the EDGES low band measurements to study constraints on the primordial magnetic field in the presence of DM-baryonic interaction. Various other observations such as the CMBR, the Sunyaev-Zel'dovich effect, the star formation, blazar light curve have been exploited to constrain the primordial magnetic field (Planck Collaboration et al., 2016a; Saga, Tashiro, and Yokoyama, 2020; Minoda et al., 2017; Marinacci and Vogelsberger, 2016; Takahashi et al., 2013). In addition, we explore the redshift evolution of the primordial magnetic field during the dark ages and cosmic dawn. The differential brightness temperature in the EDGES absorption profile starts increasing at redshift $z \sim 16$ which suggests that heating of the IGM started around that redshift. Here, we also investigate if primordial magnetic heating is able to explain this behavior. Our analysis also allows us to study the constraints on the mass of the DM particle and the interaction cross-section in presence of the primordial magnetic field.

We start with a brief discussion and essential equations regarding the heating due to the primordial magnetic field and heating/cooling due to the interactions between dark-matter and baryons. We then present our results on redshift evolution of IGM temperature and ionization fraction in presence of the primordial magnetic field, DM-baryon interaction, and the combined impact in sections 2.4, 2.3 and 2.5 respectively. We discuss constraints on the dark-matter mass and interaction cross-section in section 2.6 and present summary in section 2.7.

2.1 Energy deposition due to primordial magnetic field

Magnetic field exerts Lorentz force on the ionized component of the IGM. This causes rise in the IGM temperature, T_g. There are mainly two processes namely the ambipolar diffusion and decaying turbulence by which the magnetic field can heat up the IGM during the cosmic dawn and dark ages. We follow the prescription presented in Sethi and Subramanian (2005) and Chluba et al. (2015) to calculate the rate of heating due to these two processes. The heating rate (in unit of energy per unit time per unit volume) due to the ambipolar diffusion is given by,

$$\Gamma_{\rm AD} = \frac{(1-x_e)}{\gamma x_e \rho_b^2} \frac{\left\langle |(\nabla \times \boldsymbol{B}) \times \boldsymbol{B}|^2 \right\rangle}{16\pi^2}, \tag{2.1}$$

where $x_e = n_e/n_{\rm H}$ is the residual free electron fraction and $n_{\rm H} = n_{\rm HI} + n_{\rm HII}$. We assume $n_{\rm HII} = n_e$ as Helium is considered to be fully neutral in the redshift range of our interest. Further, ρ_b is the baryon mass density at redshift z, and the coupling coefficient between the ionized and neutral components is $\gamma = \langle \sigma v \rangle_{HH^+}/2m_H = 1.94 \times 10^{14}\,(T_g/{\rm K})^{0.375}\,{\rm cm^3 gm^{-1} s^{-1}}$. The Lorentz force can be approximated as $\left\langle |(\nabla \times \boldsymbol{B}) \times \boldsymbol{B}|^2 \right\rangle \approx 16\pi^2\,\rho_B(z)^2\,l_d(z)^{-2} f_L(n_B+3)$ (Chluba et al., 2015), where $\rho_B(z) = |{\bf B}|^2/8\pi$ is the magnetic field energy density at redshift z, $f_L(p) = 0.8313[1 - 1.02 \times 10^{-2} p] p^{1.105}$, and $l_d^{-1} = (1+z)\,k_D$. The damping scale is given by $k_D \approx 286.91\,(B_0/{\rm nG})^{-1}\,{\rm Mpc}^{-1}$ (Kunze and Komatsu, 2014). We note that the above heating rate is inversely proportional to the coupling coefficient γ and the residual electron fraction x_e. Furthermore, both γ and the ionization fraction, x_e get suppressed when the IGM is colder compared to the standard scenario. As a result, the ambipolar heating rate becomes more efficient during the cosmic dawn and dark ages.

The heating rate due to the decaying turbulence is described by,

$$\Gamma_{\rm DT} = \frac{3m}{2} \frac{\left[\ln\left(1+\frac{t_i}{t_d}\right)\right]^m}{\left[\ln\left(1+\frac{t_i}{t_d}\right) + \frac{3}{2}\ln\left(\frac{1+z_i}{1+z}\right)\right]^{m+1}} H(z)\,\rho_B(z), \tag{2.2}$$

where $m = 2\,(n_B+3)/(n_B+5)$, and n_B is the spectral index corresponding to the primordial magnetic field. The physical decay time scale (t_d) for turbulence and the time

(t_i) at which decaying magnetic turbulence becomes dominant are related as (Chluba et al., 2015),

$$t_i/t_d \simeq 14.8(B_0/\mathrm{nG})^{-1}(k_D/\mathrm{Mpc}^{-1})^{-1}. \tag{2.3}$$

The heating rate due to the decaying turbulence is more efficient at early times as it is proportional to the Hubble rate, $H(z)$, and the primordial magnetic energy density. The effect monotonically decreases at lower redshifts and becomes sub-dominant during the cosmic dawn and dark ages.

It is often assumed that, like the CMBR energy density, the primordial magnetic field and energy density scale with redshift z as $B(z) = B_0(1+z)^2$ and $\rho_B(z) \sim (1+z)^4$ respectively under magnetic flux freezing condition. However, the magnetic field energy continuously gets transferred to the IGM through the ambipolar diffusion and decaying turbulence processes. For the magnetic field with $B_0 \gtrsim 1\,\mathrm{nG}$, the transfer may be insignificant compared to the total magnetic field energy and the above scalings holds. However, this may not be a valid assumption for lower magnetic field, $B_0 \lesssim 0.1$ nG. Therefore, we self-consistently calculate the redshift evolution of the magnetic field energy using the following equation,

$$\frac{d}{dz}\left(\frac{|\boldsymbol{B}|^2}{8\pi}\right) = \frac{4}{1+z}\left(\frac{|\boldsymbol{B}|^2}{8\pi}\right) + \frac{1}{H(z)\,(1+z)}(\Gamma_{\rm DT} + \Gamma_{\rm AD}). \tag{2.4}$$

The first term in the right hand side of the above equation quantifies the effect due to the adiabatic expansion of universe, and the second term quantifies the loss of the magnetic energy due to the IGM heating due to the processes described above.

2.2 Dark matter-baryon interaction

As mentioned before, it has been shown in a few recent studies that the interactions between the cold dark matter particles and baryons could help the IGM to cool faster than the standard adiabatic cooling (Barkana, 2018; Berlin et al., 2018; Muñoz and Loeb, 2018; Liu et al., 2019). In our analysis, we consider this kind of interaction between the cold DM particles and baryons to explain the unusually strong absorption signal found by the

EDGES experiments (Barkana, 2018). We adopt the Rutherford-like velocity-dependent interaction model presented in Muñoz, Kovetz, and Ali-Haïmoud (2015) where the interaction cross-section depends on the dark matter-baryon relative velocity as $\sigma = \sigma_0(v/c)^{-4}$. The dark matter-baryon interaction models are highly constrained by structure formation (Boehm and Schaeffer, 2005), primordial nucleosynthesis and cosmic rays (Cyburt et al., 2002), CMB anisotropy (Dvorkin, Blum, and Kamionkowski, 2014), spectral distortions Ali-Haïmoud, Chluba, and Kamionkowski (2015); Diacoumis and Wong (2017), galaxy clusters Chuzhoy and Shapiro (2006); Hu and Lou (2008); Qin and Wu (2001), gravitational lensing Natarajan et al. (2002); Markevitch et al. (2004), thermal history of the intergalactic medium Muñoz and Loeb (2017); Cirelli, Iocco, and Panci (2009), 21-cm observations (Tashiro, Kadota, and Silk, 2014), and so on. We note that our model satisfies the current limits (Xu, Dvorkin, and Chael, 2018; Slatyer and Wu, 2018) given on the elastic scattering cross-section between dark matter and baryons using the measurements of CMB temperature and polarization power spectra by the Planck satellite (Planck Collaboration et al., 2016b), and the Lyman-α forest flux power spectrum by the Sloan Digital Sky Survey (SDSS) (McDonald et al., 2006).

The energy transfer rate from dark matters to baryons due to such interactions can be modeled as Muñoz, Kovetz, and Ali-Haïmoud (2015),

$$\frac{dQ_b}{dt} = \frac{2m_b\rho_\chi\sigma_0 e^{-r^2/2}(T_\chi - T_g)k_B c^4}{(m_b+m_\chi)^2\sqrt{2\pi}u_{th}^3} + \frac{\rho_\chi}{\rho_m}\frac{m_\chi m_b}{m_\chi+m_b}V_{\chi b}\frac{D(V_{\chi b})}{c^2}. \tag{2.5}$$

Similarly, the heating rate of the DM, $\dot{Q}_\chi$ can be obtained by just replacing $b \leftrightarrow \chi$ in the above expression due to symmetry. Here, m_χ, m_b and ρ_χ, ρ_b are the masses and energy densities of dark matter and baryon respectively. We can see from equation (2.5) that the heating rate is proportional to the temperature difference between two fluids i.e. $(T_\chi - T_g)$. The second term in equation (2.5) arises due to the friction between dark matter and baryon fluids as they flow at different velocities. Hence both the fluids get heated up depending on their relative velocity $V_{\chi b}$ and the drag term $D(V_{\chi b})$, given as,

$$\frac{dV_{\chi b}}{dz} = \frac{V_{\chi b}}{1+z} + \frac{D(V_{\chi b})}{H(z)(1+z)} \tag{2.6}$$

and

$$D(V_{\chi b}) = \frac{\rho_m \sigma_0 c^4}{m_b + m_\chi} \frac{1}{V_{\chi b}^2} F(r). \tag{2.7}$$

The variance of the thermal relative motion of dark matter and baryon fluids $u_{th}^2 = k_B(T_b/m_b + T_\chi/m_\chi)$ and $r = V_{\chi b}/u_{th}$. The function $F(r)$ is given by

$$F(r) = erf\left(\frac{r}{\sqrt{2}}\right) - \sqrt{\frac{2}{\pi}} r e^{-r^2/2}. \tag{2.8}$$

We see that $F(r)$ grows with r, $F(0) = 0$ when $r = 0$ and $F(r) \to 1$ when $r \to \infty$. This ensures that the heating due to the friction is negligible when the relative velocity $V_{\chi b}$ is smaller compared to the thermal motion of dark matter and baryon fluid u_{th}. However, it can be significant if $V_{\chi b}$ is higher than u_{th}. The evolution of the DM temperature T_χ can be calculated using,

$$\frac{dT_\chi}{dz} = \frac{2T_\chi}{1+z} - \frac{2}{3k_B} \frac{\dot{Q}_\chi}{H(z)\,(1+z)}. \tag{2.9}$$

The first and second terms on the r.h.s quantify the adiabatic cooling and heating rate per dark matter particle due to its interactions with baryons respectively.

We see from equations (1.9) and (2.5), that the IGM temperature becomes velocity ($V_{\chi b}$) dependent as soon as the dark matter-baryon interaction is taken into consideration which, in turn, modifies the brightness temperature T_{21}. Therefore, the observable global HI 21-cm brightness temperature is calculated by averaging over the velocity $V_{\chi b}$ as,

$$\langle T_{21}(z) \rangle = \int d^3 V_{\chi b} T_{21}(V_{\chi b}) P(V_{\chi b}), \tag{2.10}$$

where the initial velocity $V_{\chi b,0}$ follows the probability distribution

$$P(V_{\chi b,0}) = \frac{e^{-3V_{\chi b,0}^2/(2V_{\rm rms}^2)}}{(\frac{2\pi}{3} V_{\rm rms}^2)^{3/2}}. \tag{2.11}$$

In order to calculate the velocity averaged IGM temperature $\langle T_g(z) \rangle$ and ionization fraction $\langle x_e \rangle$, the same procedure is followed.

We simultaneously solve equations (1.7), (1.9), and (2.4 – 2.9) to get the evaluations in T_g and x_e for a range possible values of the dark matter particle mass m_χ, the interaction cross-section $\sigma_{45} = \frac{\sigma_0}{10^{-45}\,\mathrm{m}^2}$, and the initial magnetic field (B_0) for a given $V_{\chi b}$. We

then use eq. 2.10 to calculate the averaged quantities such as, $\langle T_{21}(z)\rangle$, $\langle T_g(z)\rangle$ and $\langle x_e\rangle$. Note that all values/results quoted below are these average quantities even if we don't mention them explicitly. Below we discuss our results on the heating due to the primordial magnetic field, the impacts of the DM-baryonic interaction in presence/absence of the magnetic field. In addition, we present our studies on the role of the residual free electron fraction x_e in the context of the colder IGM background, the evolution of the primordial magnetic field, and the upper limit on the primordial magnetic field using EDGES absorption profile. We set the following initial conditions at redshift $z_i = 1010$: $T_{\rm gi} = 2.725(1+z_i)\,{\rm K}$; $T_{\chi i} = 0$, $V_{\chi b,i} = V_{\rm rmsi} = 29\,{\rm km/s}$, $B_i = B_0(1+z_i)^2$ and $x_{ei} = 0.055$ (obtained from RECFAST code[†] Seager, Sasselov, and Scott, 1999; Seager, Sasselov, and Scott, 2000).

2.3 Impact on heating due to the primordial magnetic field

The upper panel of Fig. 2.1 shows the evolution of IGM temperature T_g in presence of the primordial magnetic field with $B_0 = 0.05\,{\rm nG}$ and $0.5\,{\rm nG}$. We fix $n_B = -2.9$ throughout our analysis. In order to understand the role of the primordial magnetic field alone we do not include the DM-baryon interaction in Fig. 2.1. Note that our results for $B_0 = 3\,{\rm nG}$ and Hydrogen only scenario is very similar to that presented in Chluba et al. (2015) for the similar scenario. We find that the primordial magnetic field makes a noticeable change in the IGM temperature during the cosmic dawn and dark ages ($z \lesssim 100$) for $B_0 \gtrsim 0.03\,{\rm nG}$. This is because the ambipolar diffusion becomes very active at lower redshifts as it is inversely proportional to the square of the baryon density, ρ_b. It also scales with the IGM temperature as $T_g^{-0.375}$ (see eq. 2.1). The Effects due to the decaying turbulence, which scales as $\Gamma_{DT} \propto H(z)\,\rho_B(z)$, get diluted at lower redshifts. We find that for $B_0 \sim 0.1\,{\rm nG}$, the IGM temperature rises to the CMBR temperature and, consequently, the global differential brightness temperature T_{21} becomes nearly

[†]http://www.astro.ubc.ca/people/scott/recfast.html

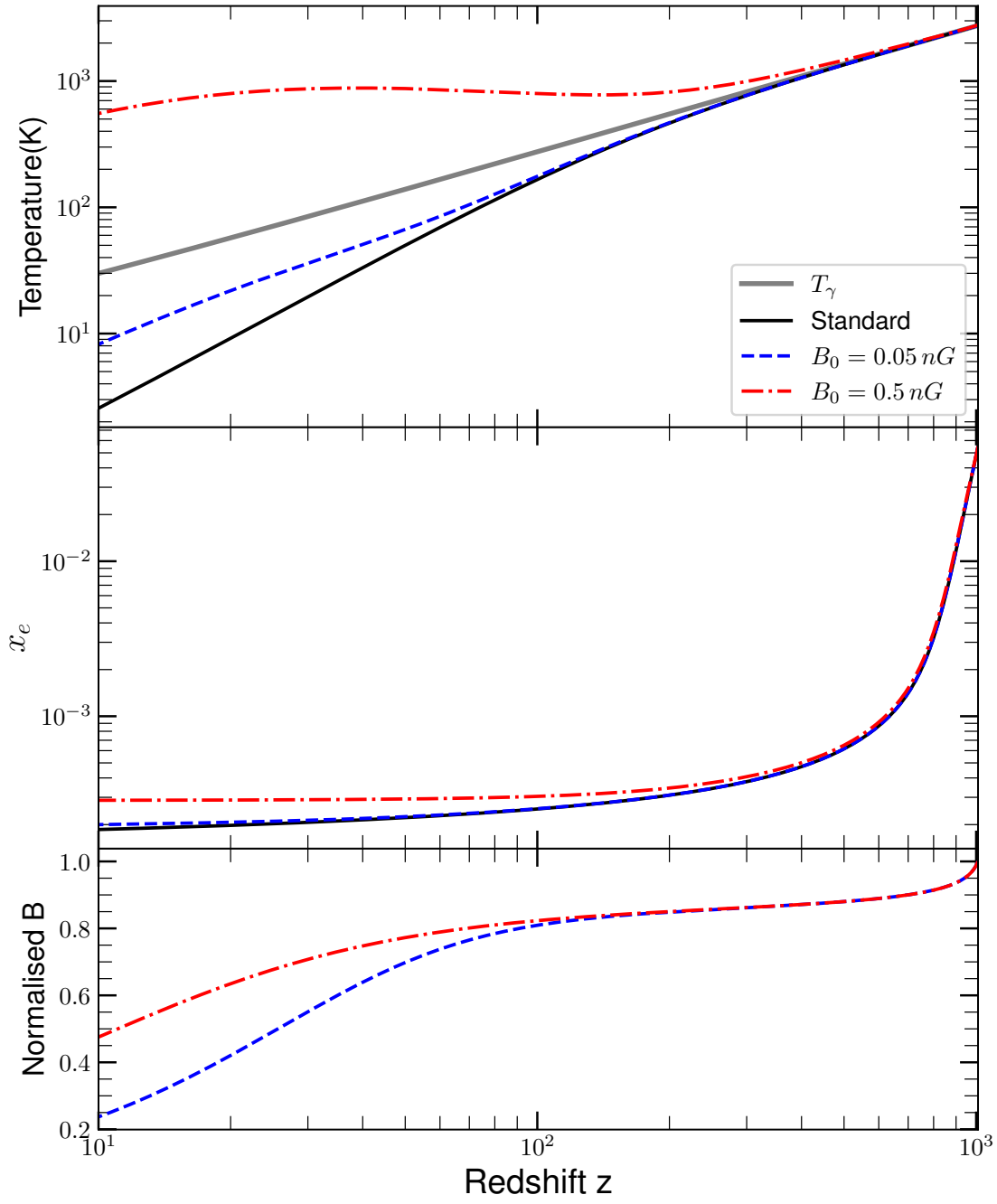

Figure 2.1: The upper and middle panels show the IGM kinetic temperature T_g and residual free electron fraction x_e as a function of redshift in presence of the primordial magnetic field. The solid (black), dashed-dotted (red) and dashed (blue) lines correspond to the primordial magnetic field with $B_0 = 0$, 0.05 and $0.5\,\mathrm{nG}$ respectively. The grey thick solid line shows the CMBR temperature T_γ. We do not include the DM-baryon interaction here. The lower panel shows the normalised magnetic field i.e. $\frac{B(z)}{B_0(1+z)^2}$ for the same B_0 values mentioned above.

zero. Further increase of the primordial magnetic field causes the IGM temperature to go above the CMBR temperature and T_{21} becomes positive. This is completely ruled out as the EDGES measured the HI 21-cm signal in absorption i.e., T_{21} is negative. This put an upper limit on the primordial magnetic field and we find $B_0 \lesssim 0.1\,\mathrm{nG}$, similar to the upper limit found by Minoda, Tashiro, and Takahashi (2019).

The middle panel of Fig. 2.1 shows the history of residual free electron fraction, x_e. We see that x_e increases if we increase the magnetic field B_0. This is because of suppression in the Hydrogen recombination rate α_e due to an increase in the IGM temperature T_g. The increase is more prominent during the cosmic dawn and dark ages. For example, x_e increases by a factor of ~ 1.5 as compared to the standard prediction at redshift $z = 17$ if $B_0 = 0.5\,\mathrm{nG}$. Conversely, the residual free electron fraction x_e directly influences the magnetic heating and its evolution through the ambipolar diffusion process (eq. 2.1 and 2.4) which is dominant over the decaying turbulence during the cosmic dawn and dark ages. Therefore it is important to highlight the role of x_e in constraining the primordial magnetic field using the global 21-cm signal. Moreover, x_e also affects the standard Compton heating (see eq. 1.9).

The bottom panel of Fig. 2.1 shows the evolution of the primordial magnetic field. The normalised primordial magnetic field ($\frac{B(z)}{B_0(1+z)^2}$) has been plotted here to highlight any departure from the simple $B_0(1+z)^2$ scaling. We find that the primordial normalised magnetic field maintains a constant value at higher redshifts $z \gtrsim 100$, and then decays at lower redshifts during the cosmic dawn and dark ages as a considerable fraction of the magnetic field energy is transferred to the IGM for its heating through the ambipolar diffusion process. The ambipolar diffusion becomes very active at lower redshifts for reasons explained in subsection 2.1. We also notice that the amount of decay of the magnetic field depends on B_0. For example, the normalised primordial magnetic field goes down to ~ 0.4 and ~ 0.6 for $B_0 = 0.05\,\mathrm{nG}$ and $0.5\,\mathrm{nG}$ at redshift $z \sim 17.2$. This implies that the fractional decay of the magnetic energy is more when the primordial magnetic field is weaker. For a higher primordial magnetic field with $B_0 \gtrsim 1\,\mathrm{nG}$, the

fractional decay is not significant and it can be safely assumed to scale as $(1+z)^2$.

2.4 Effect of dark matter-baryon interaction

We consider the DM-baryon interaction model that was discussed in Sec. 2.2. As mentioned there, the model has two free parameters i.e., the mass of the dark matter particle, m_χ and the interaction cross-section between the dark matter particles and baryons, σ_{45}. Below we briefly discuss the impact of the DM-baryon interaction on the IGM temperature, T_g, and residual free electron fraction, x_e. We refer readers to Datta et al. (2020) for a more elaborate discussion.

The upper panel of Fig. 2.2 shows the evolution of IGM temperature for two sets of dark matter mass m_χ and interaction cross-section σ_{45} i.e., $(1\,\mathrm{GeV},\ 1)$ and $(0.01\,\mathrm{GeV},\ 50)$. We also plot the IGM temperature as predicted in the standard model. As expected, the interaction helps the IGM to cool faster and the IGM temperature becomes lower than the standard scenario during the cosmic dawn. Lower the dark matter mass, m_χ and/or larger the cross-section σ_{45}, more the rate of IGM cooling is and, consequently, lower the IGM temperature. We note that for higher cross-section σ_{45}, the IGM temperature gets decoupled from the CMBR temperature early and coupled to the dark matter temperature T_χ. This helps the IGM and the dark matter to reach the thermal equilibrium. After that, both the IGM and dark matter temperatures scale as $(1+z)^2$ which is seen at redshifts $z \lesssim 100$ for $m_\chi = 0.01\,\mathrm{GeV}$ and $\sigma_{45} = 50$ (the blue-dashed curve in Fig. 2.2). Here we note that there are mainly two effects arising due to the interaction between the cold DM and baryon. First, it helps to cool down the IGM faster (first term of r.h.s. of eq. 2.5). Second, the friction due to the relative velocity between the DM and baryon can heat up both the DM and IGM (second term of r.h.s. of eq. 2.5). We find that the friction heating dominates over the cooling for the DM particle mass $m_\chi \gtrsim 1\,\mathrm{GeV}$, and instead of cooling, the IGM gets heated due to the DM-baryon interaction for higher DM particle mass. However, in our case, we need faster cooling off the IGM. Therefore, friction heating always remains subdominant in our case. The bottom panel of Fig. 2.2

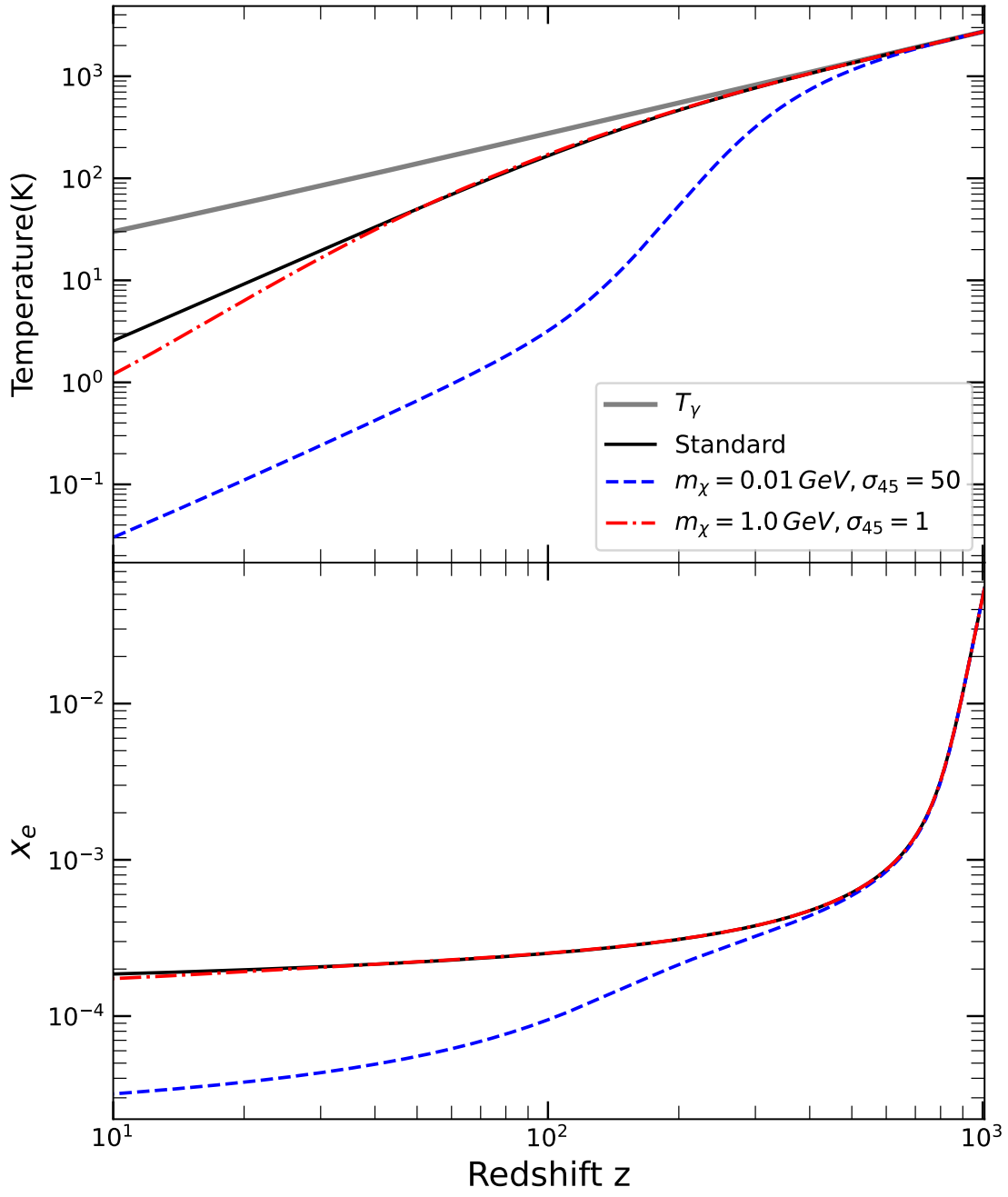

Figure 2.2: The upper and lower panels show the IGM kinetic temperature, T_g and residual free electron fraction, x_e as a function of redshift when the DM-baryon interaction is considered. The solid (black), dashed (blue), and dashed-dotted (red) lines correspond to $(m_\chi/\mathrm{GeV},\ \sigma_{45}) = (0, 0),\ (0.01, 50)$ and $(1, 1)$ respectively. The effect due to the primordial magnetic field is absent here. The grey thick solid line represents the CMBR temperature T_γ.

shows the evolution of the residual free electron fraction, x_e. As expected the residual free electron fraction is lower when the DM-baryon interaction comes into play. This is because the Hydrogen recombination rate α_e is increased when the IGM temperature is lower. The change in x_e is not significant for $m_\chi = 1$ GeV and $\sigma_{45} = 1$ (red curve). However, x_e is reduced by factor of ~ 5 for $m_\chi = 0.01\,\mathrm{GeV}$ and $\sigma_{45} = 50$ (blue curve). The reduced x_e enhances the rate of IGM heating through the ambipolar diffusion. At the same time, lower IGM temperature reduces the coupling co-efficient $\gamma(T_g)$ (eq. 2.1), which again enhances the heating rate. Moreover, heating due to the Compton process, which is proportional to $x_e(T_\gamma - T_g)$ (second term on the rhs of eq. 1.9), gets affected when the IGM is colder compared to the standard scenario.

2.5 Combined impact of primordial magnetic field and dark matter-baryon interaction

Here we discuss results on the combined impact of the primordial magnetic field and DM-baryon interaction on the IGM temperature evolution. Fig. 2.3 shows the evolution of the IGM temperature when both the primordial magnetic field and DM-baryon interactions are considered. In Table 2.1 we have mentioned T_{21} at $z = 17.2$ as predicted by our models with different model parameters and shown which parameter set is allowed or not allowed determined by the EDGES measurements. We see that the differential brightness temperature T_{21} at $z = 17.2$, for the parameter set $m_\chi = 0.001\,\mathrm{GeV}$, $\sigma_{45} = 30$, is within the allowed range when the primordial magnetic field with B_0 as high as $B_0 = 0.4\,\mathrm{nG}$ is active, although T_{21} is much lower when the magnetic field is kept off. Similarly, the parameter set $m_\chi = 0.1\,\mathrm{GeV}$, $\sigma_{45} = 5$ is ruled out as it predicts much lower T_{21} than what is allowed by the EDGES data. However, if we include the primordial magnetic field, say, $B_0 = 0.1\,\mathrm{nG}$, the above parameter set becomes allowed. Contrary to this, T_{21} predicted by some combinations of m_χ, σ_{45} could be well within the allowed range when there is no primordial magnetic field, but ruled out when the magnetic field is applied. For example $T_{21} = -0.62\,\mathrm{K}$ for $m_\chi = 1\,\mathrm{GeV}$, $\sigma_{45} = 1$ when

Table 2.1: The table shows the globally averaged differential brightness temperature T_{21} at redshift $z = 17.2$ for various set of the model parameters m_χ, σ_{45} and B_0. The allowed range of T_{21} at redshift $z = 17.2$ as measured by the EDGES is $-0.3\,\mathrm{K}$ to $-1.0\,\mathrm{K}$.

m_χ (GeV)	σ_{45}	B_0 (nG)	T_{21} (K)	Allowed
×	×	×	-0.22	×
×	×	0.1	0.00	×
0.1	5	0.1	-0.87	√
1.0	1	×	-0.62	√
1.0	1	0.05	-0.15	×
0.001	300	0.4	-0.33	√
0.1	50	0.1	-1.08	×

$B_0 = 0$, but goes to $-0.15\,\mathrm{K}$ which is above the allowed range for $B_0 = 0.05\,\mathrm{nG}$.

We discussed in section 2.3 that the primordial magnetic field with $B_0 \gtrsim 0.1\,\mathrm{nG}$ is ruled out in the standard scenario, but it can be well within the allowed range when the interaction between DM and baryon with an appropriate parameter sets comes into play. In general, we find that the exact upper limit on the primordial magnetic field depends on the mass of the DM particles m_χ and the DM-baryonic interaction cross-section σ_{45}. We see that the primordial magnetic field with $B_0 \sim 0.4\,\mathrm{nG}$ is allowed for an appropriate set of m_χ and σ_{45}. Note that this primordial magnetic field is ruled out in the standard scenario.

The upper panel of Fig. 2.3 shows that the primordial magnetic field and DM-baryonic interaction together introduces a 'plateau-like feature' in the redshift evolution of the IGM temperature for a certain range of model parameters m_χ, σ_{45} and B_0. One such example can be seen for $m_\chi = 0.01\,\mathrm{GeV}$, $\sigma_{45} = 50$ and $B_0 = 0.25\,\mathrm{nG}$ where the plateau like feature is seen in redshift range $\sim\ 50 - 150$. The cooling rate due to the DM-baryonic interaction and heating rate due to the primordial magnetic field compensates each other for a certain redshift range which gives the plateau-like feature. At lower redshifts, the heating due to the primordial magnetic field, which scales as $B^4(z)$, becomes ineffective as the primordial magnetic field decays very fast. This is both due to the adiabatic expansion of universe and loss of the magnetic energy due to heating. We notice that this plateau-like feature is not so prominent for lower primordial magnetic field. The 'plateau-like feature' is a unique signature of the DM-baryonic interaction in presence of the primordial magnetic field. However, it can only be probed by space-based experiments as it appears at redshift range $\sim 50 - 150$.

The middle and lower panels of Fig. 2.3 show the residual electron fraction, x_e, and primordial magnetic field, $B(z)$ as a function of redshift respectively. Like in previous cases, the residual electron fraction x_e is suppressed when both the DM-baryonic interactions and primordial magnetic field are active. The suppressed residual electron fraction enhances the heating rate occurring due to the ambipolar diffusion. The primordial

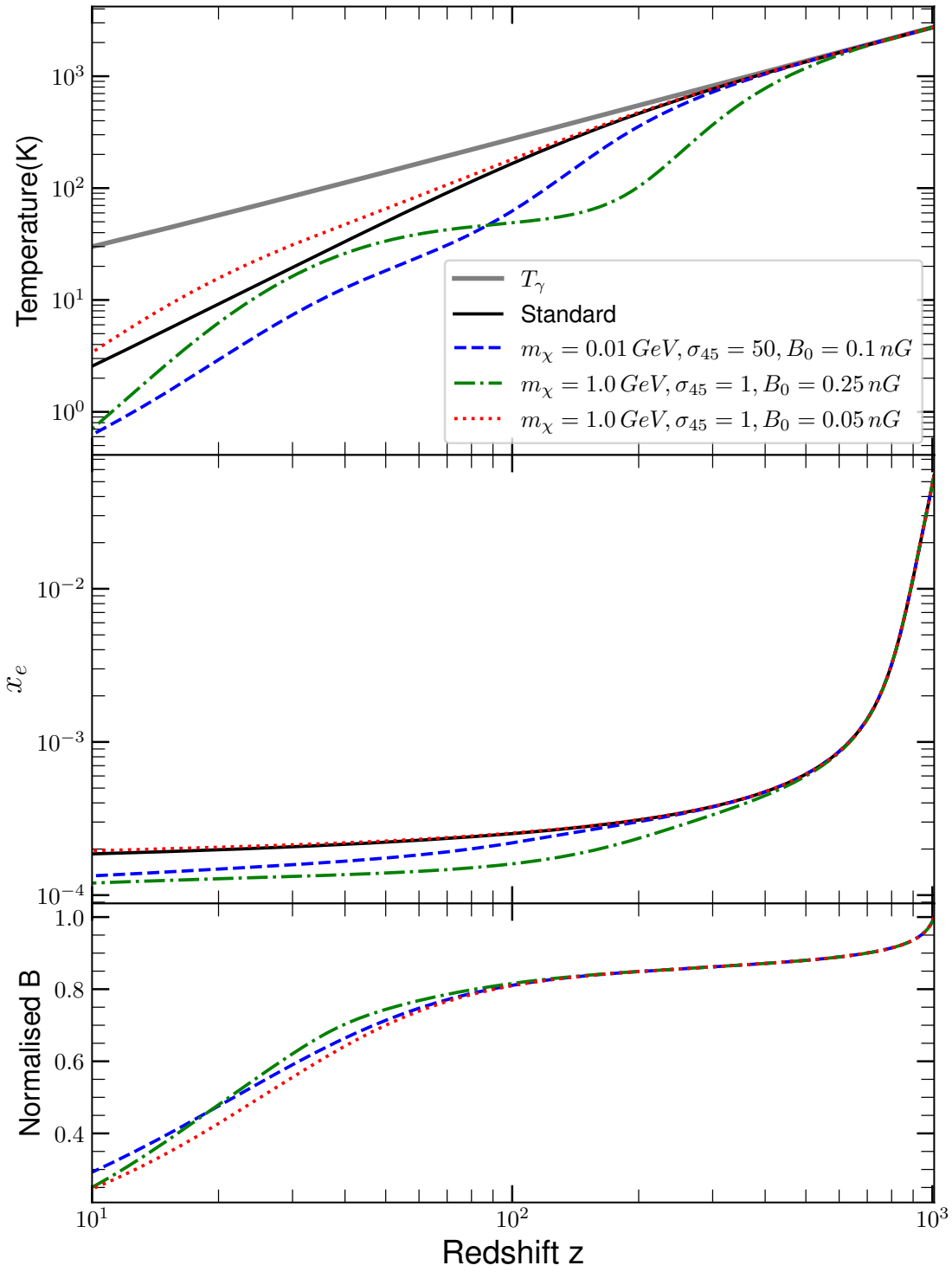

Figure 2.3: Same as Fig. 2.1, however both the primordial magnetic field and DM-baryon interaction are considered here.

magnetic field loses its energy (other than the adiabatic loss because of the expansion of universe) due to the transfer of energy to IGM heating through the ambipolar diffusion process. This loss starts becoming important at lower redshifts $z \lesssim 100$. As the primordial magnetic field decays very fast, the magnetic heating becomes ineffective at lower redshifts. The EDGES absorption spectra show that the IGM temperature is rising at redshifts $z \lesssim 17$. There are several possible mechanisms by which the IGM can be heated up such as heating due to soft X-ray, Ly-α, DM decay/annihilation (Pritchard and Furlanetto, 2007; Ghara, Choudhury, and Datta, 2015; Ghara and Mellema, 2020; Sethi, 2005; Furlanetto, Oh, and Pierpaoli, 2006; Liu and Slatyer, 2018). However, we find that the primordial magnetic field is not able to considerably heat up the IGM at the later phase of the cosmic dawn and, therefore, can not explain the heating part of the EDGES absorption profile.

2.6 Constraints on dark matter-baryon interaction in presence of the primordial magnetic field

We now provide the constraints on the allowed ranges of the dark-matter mass and interaction cross-section using EDGES observation. Fig. 2.4 demonstrates the constraints on the DM-baryon interaction in presence of the primordial magnetic field. The top left panel presents constraints on the model parameters m_χ and σ_{45} when there is no magnetic field i.e., $B_0 = 0$. This is quite similar to constraints obtained by Barkana (2018). Note that the constraints are obtained by restricting the differential brightness temperature T_{21} within $-0.3\,\mathrm{mK}$ to $-1.0\,\mathrm{K}$ as suggested by the EDGES measurements. The DM particle with mass higher than a few GeV is ruled out because the cooling due to the DM-baryonic interaction becomes inefficient and the drag heating due to the friction between the DM and baryon starts to dominate for higher DM particle mass. Therefore, the drag heating is found to have a very negligible role in the case considered here. The top right, bottom left and the bottom right panels show constraints on the model parameters m_χ and σ_{45} in presence of the primordial magnetic field with $B_0 = 0.05,\ 0.1$ and

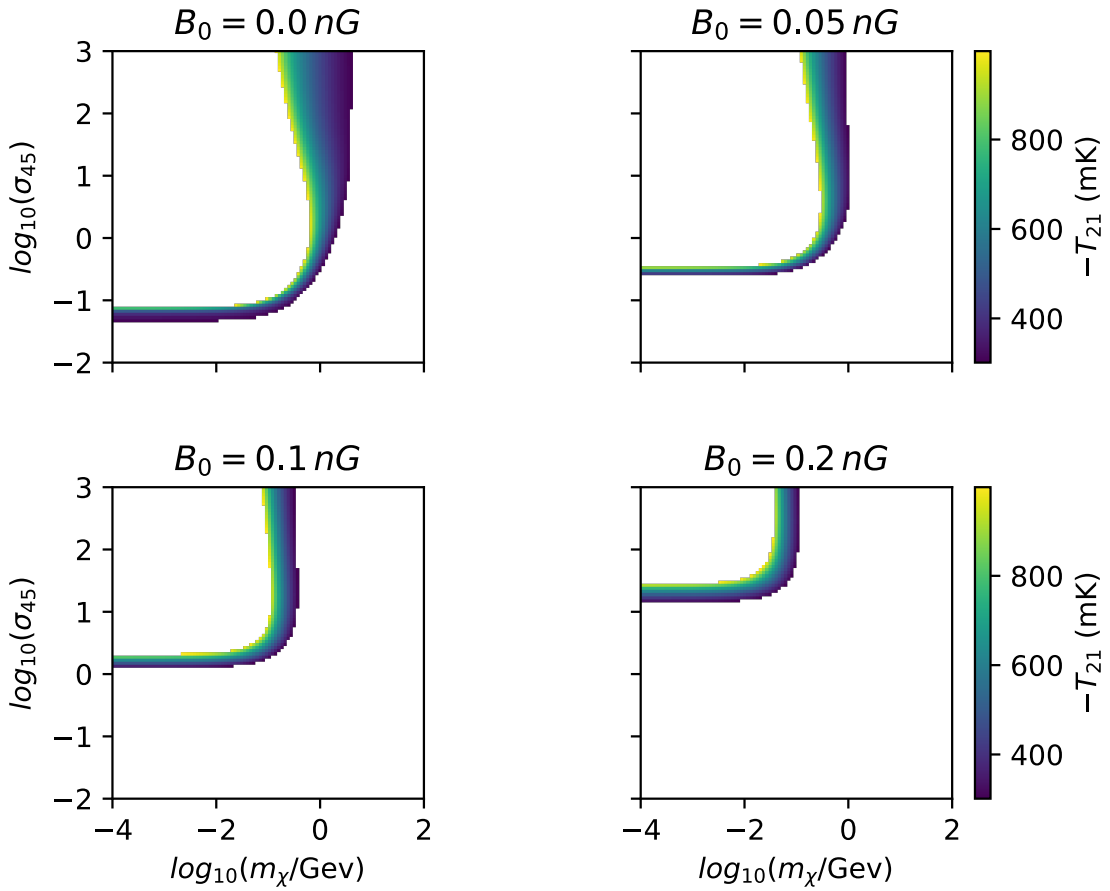

Figure 2.4: Bounds on dark matter mass, m_χ and interaction cross-section, σ_{45} in presence of the primordial magnetic field considering the constraints on T_{21} given by EDGES. As the amplitude of magnetic field, B_0 increases, the allowed dark-matter mass decreases and cross-section increases. The colour bar denotes the allowed T_{21} constrained by EDGES experiment.

$0.2\,\mathrm{nG}$ respectively. We see that the allowed range of the DM-baryon cross-section σ_{45} gradually increases as B_0 is increased. For example, the lowest allowed σ_{45} moves up, from $\sim 4 \times 10^{-47}\,\mathrm{m}^2$, to $\sim 2.5 \times 10^{-46}\,\mathrm{m}^2$, $\sim 1.5 \times 10^{-45}\,\mathrm{m}^2$ and $\sim 1.5 \times 10^{-44}\,\mathrm{m}^2$ for $B_0 = 0.05,\ 0.1$ and $0.2\,\mathrm{nG}$ respectively. On the other hand, the maximum allowed mass of the DM particle m_χ gradually decreases for higher magnetic field. In Fig. 2.4 we find that the highest allowed m_χ goes down, from $\sim 5\,\mathrm{GeV}$, to $\sim 1\,\mathrm{GeV}$, $\sim 0.3\,\mathrm{GeV}$ and $\sim 0.1\,\mathrm{GeV}$ for $B_0 = 0.05,\ 0.1$ and $0.2\,\mathrm{nG}$ respectively. The primordial magnetic field heats up the IGM and the heating is more for higher values of B_0. The DM-baryonic interaction needs to be more efficient to compensate for this extra heating which can be achieved either by increasing the cross-section σ_{45} or/and lowering the mass of the dark-matter particle m_χ.

The above discussion also tells that the exact upper limit on the primordial magnetic field parameter B_0 depends on the mass m_χ and the cross-section σ_{45}. Higher primordial magnetic field is allowed if σ_{45} is increased and/or m_χ is decreased. We see that the primordial magnetic field with $B_0 \sim 0.4\,\mathrm{nG}$ (Table 2.1) is allowed for an appropriate set of m_χ and σ_{45}. Note that $B_0 \gtrsim 0.1\,\mathrm{nG}$ is ruled out in the standard scenario. However, we find that the primordial magnetic field with $B_0 \gtrsim 1\,\mathrm{nG}$ may not be allowed as this requires very efficient cooling of the IGM which is unlikely even for very high cross-section and lower DM particle mass. Although, we note that a recent study by Bhatt, Jitesh R. et al. (2020), which has used the EDGES measurements, finds an upper limit of $\sim 10^{-6}\,\mathrm{G}$ on the primordial magnetic field for $m_\chi \lesssim 10^{-2}\,\mathrm{GeV}$ in presence of the DM-baryonic interaction.

2.7 Summary

Our analysis demonstrates the prospects of constraining the primordial magnetic field in light of the EDGES low band 21-cm absorption spectra during the cosmic dawn. Our study is carried out on the background of 'colder IGM' which is a promising avenue to explain the strong absorption signal found by the EDGES. We consider an interac-

tion between baryons and cold DM particles which makes the IGM colder than in the standard scenario. The primordial magnetic field heats up the IGM through the ambipolar diffusion and decaying turbulence which, in turn, influences the 21-cm differential brightness temperature. We highlight the role of the residual electron fraction. We also study constraints on the DM-baryon interaction in presence of the primordial magnetic field, features in the redshift evolution of IGM temperature. In addition, we consider the redshift evolution of the primordial magnetic field during dark ages and cosmic dawn. In particular, we focus on the departure from the simple adiabatic scaling of the primordial magnetic field (i.e. $B(z) \propto (1+z)^2$) due to the transfer of magnetic energy to the IGM.

Studying the role of the primordial magnetic field on the background of colder IGM is important for several reasons. First, it suppresses the abundance of the residual free electron fraction x_e (Datta et al., 2020) which, in turn, enhances the rate of IGM heating through the ambipolar diffusion. Second, the coupling coefficient between the ionized and neutral components $\gamma(T_g)$ decreases with the IGM temperature, which again results in the increased heating rate (see eq. 2.1). Third, the heating rate due to the Compton process, which is proportional to $(T_\gamma - T_g)$ and x_e, too gets affected when the background IGM temperature T_g is lower (eq. 1.9). We find that collectively all these effects make the heating rate due the magnetic field faster in the colder background in comparison to the heating rate in the standard scenario. Consequently, the primordial magnetic field decays, with redshift, at a much faster rate compared to the simple $(1+z)^2$ scaling during the dark ages and cosmic dawn. The decay is particularly significant for $B_0 \lesssim 0.5\,\mathrm{nG}$ when the fractional change in the magnetic field due to the heating loss could be $\sim 50\%$ or higher. This is unique in the colder IGM scenario.

Next, we find that the upper limit on the primordial magnetic field using the EDGES measurements is determined by the underlying non-standard cooling process, i.e., the DM-baryon interaction here. Higher primordial magnetic field may be allowed when the underlying DM-baryon interaction cross section is higher and/or the DM particle mass is lower, i.e., the exact upper limit on B_0 depends on the DM mass and the interaction

cross-section. For example, the primordial magnetic filed with $B_0 \sim 0.4\,\mathrm{nG}$ which is ruled out in the standard model (Minoda, Tashiro, and Takahashi, 2019), may be allowed if the DM-baryon interaction with $m_\chi = 0.01\,\mathrm{GeV}$ and $\sigma_{45} = 100$ is included. However, we find that the primordial magnetic field with $B_0 \gtrsim 1\,\mathrm{nG}$ may not be allowed as this requires very efficient cooling of the IGM which is unlikely to occur even for very strong possible DM-baryon interaction.

Furthermore, we observe that the primordial magnetic field and DM-baryonic interaction together introduces 'a plateau-like feature' in the redshift evolution of the IGM temperature for a certain range of model parameters m_χ, σ_{45} and B_0. The cooling rate due to the DM-baryonic interaction and heating rate due to the primordial magnetic field compensates each other for a certain redshift range which produces the plateau-like feature. However, this kind of plateau is not prominent for lower primordial magnetic field with $B_0 \lesssim 0.1\,\mathrm{nG}$.

The EDGES absorption spectra suggest that the IGM temperature has possibly gone up from $\sim 3\,\mathrm{K}$ at redshift $z \approx 16$ to $\sim 40\,\mathrm{K}$ at redshift $z \approx 14.5$. There are several possible candidates such as soft X-ray photons from the first generation of X-ray binaries, mini-quasars, high energy photons from DM-decay/annihilations, primordial magnetic field, etc. which could heat up the IGM during the cosmic dawn. However, our study shows that the heating due the primordial magnetic field becomes very weak during the above redshift range. Because the magnetic energy density decreases very fast prior to the cosmic dawn both due to the adiabatic expansion of universe and the loss due to IGM heating. Therefore, it is unlikely that the primordial magnetic field contributes to the heating of the IGM during the late phase of the cosmic dawn as indicated by the EDGES measurements.

Finally, we see that the allowed DM-baryon cross-section σ_{45} gradually shifts towards higher values as B_0 is increases. On the other hand, the allowed mass of the DM particle m_χ gradually decreases for higher values of the primordial magnetic field. Because, the DM-baryon interaction needs to be more efficient to compensate for the excess

heating caused due to higher magnetic field, which can be achieved either by increasing the cross-section or lowering the mass of the Dark matter particle.

There could be various other models of the DM-baryon interactions, for which the exact upper limit on the primordial magnetic field, and all other results discussed above might change to some extent. However, the general conclusions regarding the role of the primordial magnetic field on a colder IGM background are likely to remain valid for any mechanism providing faster cooling off the IGM. We now focus on different radiation backgrounds that are generated due to the formation of first stars or early galaxies during cosmic dawn and epoch of reionization.